Int. J. Heat Mass Transfer. Vol. 37, No. 1, pp. 27–41, 1994
Printed in Great Britain

0017–9310/94 $6.00 + 0.00

Pressure gradient effects on Reynolds analogy for constant property equilibrium turbulent boundary layers

RONALD M. C. SO
Mechanical and Aerospace Engineering, Arizona State University, Tempe, AZ 85287-6106, U.S.A.

(*Received* 10 *March* 1993 *and in final form* 14 *July* 1993)

Abstract—The effects of pressure gradient on turbulent heat transfer to or from planar surfaces are examined. Only incompressible, equilibrium thermal boundary layers are investigated. The equilibrium condition is characterised by the Clauser parameter β. Temperature profiles which are parametric in β and the turbulent Prandtl number, Pr_t, have been calculated for the range $-0.54 \leqslant \beta \leqslant \infty$; corresponding in one end to a favorable pressure gradient flow beyond which no equilibrium boundary layer is possible and in the other end to turbulent flow at incipient separation, respectively. It is found that an overlap exists between the temperature law of the wall region and the outer defect law region for all values of β and Pr_t, except when $\beta \to \infty$. The existence of this overlap region gives rise to an expression for the Stanton number which is shown to be a function of β and Pr_t. At incipient separation, the skin friction coefficient goes to zero while the wall heat flux remains finite. However, the wall heat flux and the Stanton number in this limit cannot be determined because of the neglect of viscous effects in the present analysis. A modified Reynolds analogy that accounts for the effects of β and Pr_t is deduced and the classical Reynolds analogy is shown to be valid only in the limit of β goes to zero, Pr_t goes to 1 and the Reynolds number based on the displacement thickness approaches infinity.

INTRODUCTION

THE STUDY of isothermal, incompressible, equilibrium turbulent boundary layers on plane surfaces was first attempted by Clauser [1]. He pointed out that equilibrium boundary-layer flows can be established if the parameter $\beta = \delta^*(\mathrm{d}P/\mathrm{d}x)\tau_w$ is maintained constant throughout the flow. Here, $\mathrm{d}P/\mathrm{d}x$ is the streamwise pressure gradient. Clauser also showed that the outer boundary layer can be analysed by assuming an eddy viscosity K_M such that $K_M \propto U_\infty \delta^*$. The work of Clauser was later extended by Townsend [2, 3]. However, the problem was being analysed in a piecemeal fashion and the theories proposed involved a considerable amount of approximations and empiricism.

A rather complete analysis of isothermal, incompressible, equilibrium turbulent boundary layers on plane surfaces was later given by Mellor and Gibson [4]. They based their study on the well-known two-layer model for turbulent boundary layers and a derived eddy viscosity function that is valid in the entire region outside of the viscous sublayer. The extension of the eddy viscosity function to include viscous effects was given by Mellor [5] in a companion paper. In their analysis, Mellor and Gibson [4] invoked basic physical assumptions similar to those made by Townsend [2, 3]; however, the empirical information required was limited to that extracted from zero pressure-gradient flow only. Consequently, the theory is on stronger theoretical ground. Besides, Mellor and Gibson [4] demonstrated that the incipient separation profile of Stratford [6], where $\tau_w \approx 0$, was also a member of the family of equilibrium profiles obtained with β held constant. Subsequent measurements of boundary layers with zero, negative and positive pressure gradients by Kline *et al.* [7] provided further evidence to support Mellor and Gibson's [4] analysis. Their measurements showed that an overlap region indeed exists; thus giving rise to a logarithmic law of the wall and verifying the validity of the skin friction coefficient determined from the log law. Therefore, Mellor and Gibson's [4] analysis of the equilibrium layers was by far the most thorough and complete to date.

On the other hand, thermal equilibrium turbulent boundary layers have received scant attention. The most studied case is the thermal boundary layer developed on a flat plate with zero pressure gradient ($\beta = 0$) and constant freestream and wall temperatures. Some careful measurements by Reynolds *et al.* [8] and Perry *et al.* [9] showed that the temperature profiles are quite similar to the velocity profiles and, therefore, can be described by the two-layer model commonly used to analyse velocity layers. Near the wall, the temperature is determined by the fluid properties, such as density ρ, kinematic viscosity ν, thermal conductivity k, specific heat at constant pressure C_p, and the wall variables given by wall shear stress τ_w, wall heat flux q_w and the normal coordinate y measured from the wall. Dimensional arguments then lead to the temperature law of the wall,

NOMENCLATURE

A constant in the velocity defect law, defined in equation (19)
A_θ constant in the temperature defect law, defined in equation (42)
$\tilde{A}_\theta$ constant in the temperature defect law, defined in equation (4)
B constant in the velocity law of the wall, defined in equation (18)
B_θ constant in the temperature law of the wall, defined in equation (2)
C coefficient of Reynolds analogy, defined in equation (28)
C_1 constant defined in equation (49)
C_f skin friction coefficient, $2\tau_w/\rho U_e^2$
C_p specific heat at constant pressure
e root of equation given by combining (17a) and (17b)
E root of the equation given by combining (41a) and (41b)
f dimensionless velocity defect function defined for small β
F dimensionless velocity defect function defined for large β
g dimensionless temperature defect function defined for small β
G dimensionless temperature defect function defined for large β
$\tilde{G}$ defect shape factor, $\int_0^\gamma \left(\frac{U_e - U}{u_\tau}\right)^2 \mathrm{d}y \Big/ \Delta$
h channel half width
k thermal conductivity
K acceleration parameter, $\frac{\nu U_e'}{U_e^2}$
K_C constant in the definition of the outer-layer eddy viscosity, 0.016
K_H thermal eddy diffusivity
K_M eddy viscosity
m dimensionless parameter, $\frac{\Delta U_e'}{\Delta' U_e}$
Nu Nusselt number, $St\ Pr\ Re_x$
P mean pressure
Pr Prandtl number
Pr_t turbulent Prandtl number
q total heat flux
q_w wall heat flux
Re_x Reynolds number based on the stream coordinate, $U_e x/\nu$
R_{δ^*} Reynolds number based on the displacement thickness, $U_e \delta^*/\nu$
$R_{\delta^*}(0)$ Reynolds number evaluated at $x = 0$, $U_e(0)\delta^*(0)/\nu$
St Stanton number, $\frac{-q_w}{\rho C_p U_e \Theta_e}$
u fluctuating velocity along the x-direction
u_τ skin friction velocity, $\sqrt{(\tau_w/\rho)}$
u_p pressure velocity, $(\delta^*(\mathrm{d}P_e/\mathrm{d}x)/\rho)^{1/2}$
U mean velocity along x-direction
U_e freestream velocity
v fluctuating velocity along y-direction
V mean velocity along y-direction
x stream coordinate
$\tilde{x}$ normalized x coordinate, $\int_0^x \frac{\gamma}{\gamma(0)}\mathrm{d}x$
y normal coordinate.

Greek symbols
β Clauser parameter, $\delta^*(\mathrm{d}P_e/\mathrm{d}x)/\tau_w$
γ skin friction defined for small β, u_τ/U_e
δ boundary layer thickness
δ^* displacement thickness, $\int_0^\infty \frac{U_e - U}{U_e}\mathrm{d}y$
Δ defect thickness, $\int_0^\infty \frac{U_e}{u_\tau}\frac{U}{}\mathrm{d}y = \frac{\delta^*}{\gamma}$
η dimensionless y coordinate, y/Δ
η_θ dimensionless thermal boundary layer thickness
θ fluctuating temperature
Θ mean temperature difference between the fluid and the wall
Θ_τ friction temperature, $-q_w/\rho C_p u_\tau$
Θ_p pressure temperature, $C\lambda\Theta_e$
Θ_e freestream temperature
κ von Karman constant for the velocity law of the wall, 0.41
κ_θ von Karman constant for the temperature law of the wall
λ skin friction defined for large β, $\gamma\beta^{1/2}$
ν fluid kinematic viscosity
ξ stretched dimensionless y coordinate
ρ fluid density
τ total shear stress
τ_w wall shear stress
φ dimensionless eddy viscosity function defined for small β
φ_θ dimensionless eddy thermal diffusivity defined for small β, φ/Pr_t
Φ dimensionless eddy viscosity function defined for large β.

$$\frac{\Theta}{\Theta_\tau} = fn\left(\frac{yu_\tau}{\nu}, Pr\right). \tag{1}$$

Strictly speaking, the arguments leading to (1) are valid only for flow cases where there is no freestream turbulence, the freestream temperature Θ_e is small enough for the flow to be considered incompressible and the variations of fluid properties across the layer are small. If, in addition, the flow is assumed to have a constant flux region near the wall, the temperature

profile outside the viscous sublayer can be shown to be described by the logarithmic law of the wall,

$$\frac{\Theta}{\Theta_\tau} = \frac{1}{\kappa_\theta}\ln\left(\frac{yu_\tau}{\nu}\right) + B_\theta. \tag{2}$$

The value for κ_θ could be determined through classical mixing length arguments and by assuming the thermal eddy diffusivity K_H to be given by $K_H = K_M/Pr_t$. Therefore, according to Kader and Yaglom [10], κ_θ can be shown to relate to the von Karman constant κ by $\kappa_\theta = \kappa/Pr_t$. In general, B_θ is a function of Pr. For air, Kader and Yaglom [10] showed that $B_\theta = 3.8$ correlates well with flat-plate boundary layers and pipe flow heat transfer data they have examined. Besides, measurements in square duct by Brundrett and Burroughs [11] and the flat-plate boundary-layer experiment of Perry and Hoffmann [12] also lend support to (2) with $B_\theta = 3.8$. As a result, the temperature law of the wall can be taken to be given by (2) with $\kappa_\theta = \kappa/Pr_t$ and $B_\theta = 3.8$ for air.

Far away from the wall in the fully turbulent region, the temperature is nearly independent of the molecular diffusivities. However, it is affected by the boundary layer thickness, δ, and the freestream temperature, Θ_∞. Dimensional arguments again lead to

$$\frac{\Theta_\infty - \Theta}{\Theta_\tau} = fn\left(\frac{y}{\delta}\right). \tag{3}$$

If an overlap region exists, it can be easily shown that [10]

$$\frac{\Theta_\infty - \Theta}{\Theta_\tau} = -\frac{1}{\kappa_\theta}\ln\left(\frac{y}{\delta}\right) + \tilde{A}_\theta. \tag{4}$$

Kader and Yaglom [10] found that $\tilde{A}_\theta$ is different for flows in pipes, channels and boundary layers. For pipe flow, according to the data examined by Kader and Yaglom [10], $\tilde{A}_\theta \approx 0$ is found to give a good correlation between (4) and the measurements. However, for flat plate boundary layers, Kader and Yaglom [10] could not find any reliable data to determine $\tilde{A}_\theta$ with sufficient accuracy. Nevertheless, they assumed $\tilde{A}_\theta = 2.35$ based on the argument that $K_H = K_M$ in the outer region and that the dimensionless velocity and temperature profiles in this region have the same shape. If these dimensionless profiles are indeed similar, then according to the analysis of Mellor and Gibson [4], $\tilde{A}_\theta \approx 1.6$. Therefore, in spite of the detailed study of Kader and Yaglom [10] and Yaglom [13], the correct value of $\tilde{A}_\theta$, even for flat plate boundary layers, is not known. Besides, the assumption of $K_H = K_M$ in the outer region is not quite correct. The data examined by Kader and Yaglom [10] and Yaglom [13] suggest a value of $K_H = K_M/0.85$.

For flat plate boundary layers, the mean momentum and temperature equations are similar. In addition, the boundary conditions for U and Θ are identical; that is, U and Θ go to zero at the wall and approach their free stream values U_∞ and Θ_∞ at the edge of the boundary layer. If $K_H = K_M$ is assumed, the equations become identical and the same solution for velocity and temperature is obtained. This suggests that $\tilde{A}_\theta \approx 1.6$, the same as that determined from the isothermal study of Mellor and Gibson [4]. In general, K_H is not equal to K_M; therefore, a study of the equilibrium thermal boundary layer in a manner similar to that proposed by Mellor and Gibson [4] is suggested. This analysis could also be used to assess the effects of pressure gradient on heat transfer and the validity of the Reynolds analogy. However, it will be limited to cases where the aerodynamic and thermal boundary layers are in equilibrium.

Measurements on heat transfer in flows with streamwise pressure gradient are scarce [9, 13] and are essentially non-existent for situations where β = constant. Some measurements [14, 15] with accelerating external flow were available and a limited amount of decelerated flow data were also included in ref. [14]. However, the boundary layers investigated in these studies were not in equilibrium. The reason being that the acceleration parameter K specified in these studies was larger than the minimum β where equilibrium boundary layers exist [4]. For example, the smallest K specified in the study of Moretti and Kays [14] is $K \approx 0.3 \times 10^{-6}$. However, according to Mellor and Gibson [4], the smallest value of β where equilibrium accelerated boundary layers exist is $\beta = -0.54$. It can be shown that K and β are related by the expression: $K = -\beta\gamma^2/R_{\delta^*}$. Therefore, if $\beta = -0.54$ is assumed, γ is taken to be 0.035 at a $R_{\delta^*} \approx 10^4$ investigated by Moretti and Kays [14], K is estimated to be 0.7×10^{-7} which is smaller than $K \approx 0.3 \times 10^{-6}$. Other values of K investigated [14, 15] were much larger than 0.3×10^{-6}; therefore, the boundary layers studied were not in equilibrium. On the other hand, β for a fully-developed channel flow can be expressed as $(-\delta^*/h)$. Since δ^*/h is most likely less than 0.54, fully-developed turbulent channel flow is an equilibrium flow. Therefore, recent data on direct numerical simulation (DNS) of fully-developed turbulent channel flow with heat transfer [16–18] can also be considered as viable data sets besides the measurements of Perry *et al.* [9] and Yaglom [13].

In view of the present state of knowledge of thermal equilibrium boundary layers, an analytical study of such flows is warranted. Therefore, the present objectives can be stated as follows. The first objective is to investigate the family of equilibrium temperature profiles and determine their dependence on the parameters β and Pr_t. A second objective is to evaluate the correct value of $\tilde{A}_\theta$ for flat plate boundary-layer flows and the parametric variations of $\tilde{A}_\theta(\beta, Pr_t)$. Finally, the third objective is to study the validity and extent of the classical Reynolds analogy and formulate, if possible, a more general Reynolds analogy that depends on β and Pr_t. This general Reynolds analogy should approach correctly the classical Reynolds analogy in the limit of β goes to zero and Pr_t goes to 1.

FORMULATION

The flow under investigation is assumed to be two-dimensional and incompressible and Θ is considered small. Furthermore, freestream turbulence is assumed to be negligible. Under these assumptions, the governing equations are equally applicable for cooled or heated wall thermal boundary condition. Therefore, in the following analysis, no distinction will be made between these two cases. Only equilibrium flows characterised by the parameter $\beta = \text{constant}$ over smooth plane walls at constant temperature are analysed. Although the freestream velocity is allowed to vary, only flows with constant freestream temperature are considered. The analysis follows closely that of Mellor and Gibson [4]. Therefore, the governing equations for boundary-layer flows with heat transfer can be written as:

$$\frac{\partial U}{\partial x} + \frac{\partial V}{\partial y} = 0, \tag{5}$$

$$U\frac{\partial U}{\partial x} + V\frac{\partial U}{\partial y} = -\frac{1}{\rho}\frac{\mathrm{d}P}{\mathrm{d}x} + \frac{\partial}{\partial y}\left(\frac{\tau}{\rho}\right), \tag{6}$$

$$U\frac{\partial \Theta}{\partial x} + V\frac{\partial \Theta}{\partial y} = \frac{\partial}{\partial y}\left(\frac{-q}{\rho C_p}\right). \tag{7}$$

The Boussinesq definition of an eddy diffusivity is adopted, so that

$$\frac{\tau}{\rho} = \nu\frac{\partial U}{\partial y} - \overline{uv} = K_M\frac{\partial U}{\partial y}, \tag{8}$$

$$\frac{-q}{\rho C_p} = \frac{k}{\rho C_p}\frac{\partial \Theta}{\partial y} - \overline{v\theta} = K_H\frac{\partial \Theta}{\partial y}. \tag{9}$$

For boundary-layer flows, $\mathrm{d}P/\mathrm{d}x$ is given by the Bernoulli equation applied to the freestream. In other words, $-(1/\rho)(\mathrm{d}P/\mathrm{d}x) = U_\infty(\mathrm{d}U_\infty/\mathrm{d}x)$. Finally, the boundary conditions can be conveniently stated as follows:

$$V(x,0) = \Theta(x,0) = 0, \tag{10a}$$

$$\lim_{y\to 0} K_M\left(\frac{\partial U}{\partial y}\right) = \frac{\tau_w}{\rho}, \tag{10b}$$

$$\lim_{y\to 0} K_H\left(\frac{\partial \Theta}{\partial y}\right) = \frac{-q_w}{\rho C_p}, \tag{10c}$$

$$\int_0^\infty [U_\infty - U(x,y')]\,\mathrm{d}y' = \delta^*(x)U_\infty(x), \tag{10d}$$

$$\Theta(x, y\to\infty) = \Theta_\infty. \tag{10e}$$

Equations (10b,c) replace the usual no-slip conditions at the wall and simply state that the shear stress and heat flux must approach the wall shear stress and wall heat flux correctly as y goes to zero. Equation (10d) is chosen as the outer boundary condition instead of the conventional $U(x, y\to\infty) = U_\infty(x)$ because it requires the displacement thickness (and hence the momentum thickness) to be finite.

The equation set (5)–(10) can be closed by postulating diffusivity functions for K_M and K_H. In this study, $K_H = K_M/Pr_t$ is assumed and Pr_t is taken to be constant; therefore, only an eddy viscosity function for K_M is required. The assumption of a constant Pr_t is supported by the measurements of Hishida *et al.* [19] and by the DNS data of Kim and Moin [16], Kasagi *et al.* [17] and Kasagi and Ohtsubo [18]. In all these studies, Pr_t is found to be fairly constant in the fully turbulent region and its value varies from about 1 near the wall to approximately 0.8 near the pipe or channel centerline. In view of this, the constant Pr_t assumption represents a reasonable first attempt to analyse thermal equilibrium turbulent boundary layers.

Following Mellor and Gibson [4], a two-layer model with an overlap for the velocity profile is adopted. The eddy viscosity function thus proposed is given by

$$K_M = \kappa^2 y^2\left|\frac{\partial U}{\partial y}\right|, \tag{11}$$

for the inner layer, and

$$K_M = K_c\delta^* U_\infty \tag{12}$$

for the outer layer. Together, (11) and (12) give a continuous function for K_M. The dividing point between the inner and outer layer can be taken to be the larger of the two positive roots given by the solution of the equation obtained by equating (11) and (12). A value of $K_c = 0.016$ was found by Mellor and Gibson [4] to give the best overall agreement with numerous flat plate boundary-layer data they have examined.

Inherent in the analysis of Mellor and Gibson [4] is the assumption of constant shear stress in the viscous sublayer. This assumption allows the wall boundary condition (10b) to be specified and the eddy viscosity function (11) to be adopted for the analysis of the inner layer without having to account for viscous effects. In other words, their formulation neglects the viscous sublayer by bridging the fully turbulent region to the wall through a constant stress layer. Mellor and Gibson [4] found that their approach gave fairly accurate results as long as the flow Reynolds number is sufficiently large. Experimental evidence in support of such an assumption can be gleaned from the measurements of Kline *et al.* [7], where a constant stress layer was shown to exist for boundary layers in zero, negative and positive pressure gradients. A detailed consideration of the viscous sublayer and a comparative examination of the various eddy viscosity functions suitable for its analysis has been given by Mellor [5]. The present analysis adopts the approach of Mellor and Gibson [4] and further assumes that the heat flux is also constant in the viscous sublayer. Therefore, this additional assumption allows the thermal boundary condition (10c) to be specified consistent with the boundary condition (10b) for the velocity field. Besides having to limit the analy-

sis to high-Reynolds-number flows, one major advantage of the neglect of viscous effects is that there is no need to determine the relative thickness of the velocity sublayer and the thermal sublayer. In other words, the analysis can be carried out by simply assuming that the shear stress and heat flux are constant across a region defined by the larger of the velocity sublayer and the thermal sublayer depending on the thermal boundary conditions.

THE DIMENSIONLESS VELOCITY AND TEMPERATURE PROFILES

Defect solutions of the form

$$\frac{U_\infty - U}{u_\tau} = f'(\eta), \qquad \frac{\Theta_\infty - \Theta}{\Theta_\tau} = g'(\eta), \tag{13a,b}$$

are sought for the mean velocity and mean temperature profiles. With these definitions for U and Θ and the assumption of a constant turbulent Prandtl number, the following expressions can be deduced for the shear stress and the heat flux. They are

$$\frac{\tau}{\rho} = -\gamma^2 U_\infty^2 (\varphi f''), \tag{14}$$

$$\frac{-q}{\rho C_p} = -StU_\infty \Theta_\infty \left(\frac{\varphi}{Pr_t} g''\right), \tag{15}$$

where the primes applied to f and g denote differentiation with respect to η and the Stanton number St is defined as

$$St = \frac{-q_w}{\rho C_p U_\infty \Theta_\infty} = \frac{u_\tau \Theta_\tau}{U_\infty \Theta_\infty}. \tag{16}$$

The dimensionless eddy viscosity is defined by $\varphi(\eta) = K_M/\delta^* U_\infty$ while the corresponding thermal eddy diffusivity is given by $\varphi_\theta(\eta) = K_H/\delta^* U_\infty = \varphi(\eta)/Pr_t$. Thus defined, $\varphi(\eta)$ can be written in terms of f by making use of (11), (12) and (13a) and the results are:

$$\varphi(\eta) = \kappa^2 \eta^2 |f''|; \qquad \eta \leqslant e, \tag{17a}$$

$$\varphi(\eta) = K_C; \qquad \eta \geqslant e, \tag{17b}$$

where e is given by the larger of the two positive roots of the equation $\kappa^2 \eta^2 |f''| = K_C$.

According to Mellor and Gibson [4], the velocity profile away from the viscous sublayer can be described by a two-layer model; namely, the logarithmic law of the wall,

$$\frac{U}{u_\tau} = \frac{1}{\kappa} \ln \frac{y u_\tau}{\nu} + B, \tag{18}$$

and the defect law

$$\frac{U_\infty - U}{u_\tau} = -\frac{1}{\kappa} \ln \eta + A(\beta), \tag{19}$$

where $\kappa = 0.41$ and $B = 4.9$ are found to correlate well with data, and $A(\beta)$ is parametric in β. The existence of an overlap between these two regions results in a skin friction equation given by

$$\frac{1}{\gamma} = \left(\frac{2}{C_f}\right)^{1/2} = \frac{1}{\kappa} \ln \frac{\delta^* U_\infty}{\nu} + B + A(\beta), \tag{20}$$

where $\delta^* U_\infty = \Delta u_\tau$ has been substituted into (20). Furthermore, (19) and the von Karman integral equation can be used to derive the following relations

$$\frac{\gamma' U_\infty}{\gamma U'_\infty} = -\frac{\gamma/\kappa}{1+\gamma/\kappa}\left(\frac{\Delta' U_\infty}{\Delta U'_\infty} + 1\right), \tag{21}$$

$$\frac{1}{m} + 1 = \frac{\Delta' U_\infty}{\Delta U'_\infty} + 1 = -\left(1 + \frac{\gamma}{\kappa}\right) \frac{\beta^{-1} + 2 + \gamma \tilde{G}}{1 - \gamma \tilde{G} + \gamma^2 \tilde{G} \kappa^{-1}}. \tag{22}$$

The range of β in which equilibrium boundary layers exist and the particular $U(x)$ and $\Delta(x)$ distributions implied by a constant β have also been examined by Mellor and Gibson [4]. For the sake of completeness, these relations are quoted here; the interested reader should consult Mellor and Gibson [4] for details in their derivation. Equilibrium turbulent boundary layers are found to exist when the distributions of $U(x)$ and $\Delta(x)$ satisfy the following relations:

$$\frac{U_\infty}{U_\infty(0)} = \left[1 - \frac{\beta \gamma^2(0)}{m} \frac{\tilde{x}}{\delta^*(0)}\right]^m, \tag{23}$$

$$\frac{\Delta}{\Delta(0)} = \frac{\gamma(0)\delta^*}{\gamma \delta^*(0)} = \left[\frac{U_\infty}{U_\infty(0)}\right]^{1/m}. \tag{24}$$

With these distributions, the range of β in which equilibrium flow exists can be determined for a given Reynolds number. Mellor and Gibson [4] evaluated the range for $R_{\delta^*}(0) = 10^5$. They found that m is bounded by the range $-0.23 \leqslant m \leqslant -1$. The two limits correspond to $\beta = \infty$ and $\beta = -0.54$, respectively, and the physical meaning of these limits is that $\beta = \infty$ represents a flow at incipient separation while $\beta = -0.54$ represents the lower limit beyond which no equilibrium flow exists. It can be seen that the lower limit leads to the condition $\Delta U_\infty =$ constant, or the defect thickness decreases inversely as the free-stream velocity in an accelerated flow.

With these simplifications, (6) and (7) can be reduced to two third-order ordinary differential equations for f and g. The equations and the associated boundary conditions are:

$$(\varphi f'')' - \beta\left(\frac{1}{m} + 1\right) \times \left[\eta f'' - \gamma f f'' + \frac{\gamma/\kappa}{1+\gamma/\kappa}(f' + \gamma f f'' - \gamma f'^2)\right] + \beta(2f' - \gamma f'^2) = 0, \tag{25}$$

$$\left(\frac{\varphi}{Pr_t} g''\right)' - \beta\left(\frac{1}{m} + 1\right)\left[\eta g'' - \gamma f g'' + \frac{\gamma/\kappa}{1+\gamma\kappa}\left\{\left(\frac{\gamma St'}{\gamma' St} - 1\right)(g' - \gamma f' g') + \gamma f g''\right\}\right] = 0, \tag{26}$$

$$f(0) = 0, \qquad [f'(\eta)]_{\eta \to \infty} = 1, \qquad [\varphi f'']_{\eta \to 0} = -1, \tag{27a,b,c}$$

$$g(0) = 0, \qquad [g'(\eta)]_{\eta \to \infty} = 0, \qquad [\varphi g'']_{\eta \to 0} = -1, \tag{28a,b,c}$$

where the primes in γ, U_∞, Δ and St denote differentiation with respect to x.

The classical Reynolds analogy [20] for flat plate turbulent boundary layers with $K_H = K_M$ assumed can be stated as $St = \gamma^2$. However, from flat plate boundary-layer data examined by Kader and Yaglom [10], it appears that $K_H = K_M/Pr_t$ with $Pr_t = 0.85$ gives the best overall correlation between (1) and (2) and the measurements. Therefore, $St = \gamma^2$ is not quite valid, and it follows that the classical Reynolds analogy would not be suitable for heat transfer analysis with pressure gradient effects. For these flows, a general Reynolds analogy given by

$$St = C(\beta, Pr_t)\gamma^2, \tag{29}$$

where C is taken to be parametric in β and Pr_t, could be proposed. Evidence in support of this proposal can be found in the stratified flow measurements of Businger *et al.* [21] in the atmosphere and those of Arya [22] in a wind tunnel. These data were obtained in a zero pressure gradient environment. However, there is an additional body force acting on the flow due to buoyancy effects. As a result, Arya [22] showed that C depends on the bulk Richardson number, which is a dimensionless parameter characterising buoyancy effects.

Substituting (29) into (25) and (26) and integrating the equations once gives rise to two second-order ordinary differential equations for f and g. In writing down these equations, boundary conditions (27c) and (28c) have been used to evaluate the integration constants. The final equations are

$$\varphi f''' - \beta\left(\frac{1}{m}+1\right)\left[\eta f' - \left(\frac{1}{1+\gamma/\kappa}\right) f - \gamma\left(\frac{1}{1+\gamma/\kappa}\right) ff' + \gamma\left(\frac{1-\gamma/\kappa}{1+\gamma/\kappa}\right)\int_0^\eta f'\,\mathrm{d}\eta\right] + \beta\left(2f - \gamma\int_0^\eta f'^2\,\mathrm{d}\eta\right) = -1, \tag{30}$$

$$\frac{\varphi}{Pr_t} g'' - \beta\left(\frac{1}{m}+1\right)\left[\eta g' - \left(\frac{1}{1+\gamma/\kappa}\right) g - \gamma\left(\frac{1}{1+\gamma/\kappa}\right) fg' + \gamma\left(\frac{1-\gamma/\kappa}{1+\gamma/\kappa}\right)\int_0^\eta f'g'\,\mathrm{d}\eta\right] = -1, \tag{31}$$

and the remaining boundary conditions are given by (27a,b) and (28a,b). These equations are parametric in γ, β and Pr_t; therefore, they can be solved once the parameters are specified.

TRANSFORMATION FOR LARGE β

It is clear that as $\beta \to \infty$ or $\tau_w \to 0$ (flow at incipient separation), the solutions for f' and g' would increase indefinitely. Furthermore, the approximate value of η marking the edge of the boundary layer decreases as β increases. Numerically, this latter behavior is very undesirable. If the equations are to be solved properly, these singular behaviors have to be dealt with. Mellor and Gibson [4] suggested transforming the equations by re-defining a new dimensionless coordinate so that as $\beta \to \infty$ the new coordinate will also approach infinity. Consequently, the following transformation was proposed; namely

$$\eta = \xi/\beta^{1/2}, \tag{32}$$

$$f(\eta) = F(\xi), \qquad f'(\eta) = \beta^{1/2} F'(\xi), \tag{33a,b}$$

$$\gamma = \lambda/\beta^{1/2}, \qquad \tilde{G}/\beta^{1/2} = \int_0^\xi F'^2\,\mathrm{d}\xi. \tag{33c,d}$$

The physical interpretation of this transformation is that it leads to the definition of a 'pressure velocity', $u_p = [\delta^*(\mathrm{d}P/\mathrm{d}x)/\rho]^{1/2}$, which is finite. It follows that the definition of F' is given by

$$\frac{U_\infty - U}{u_p} = F'(\xi), \tag{34}$$

and (33c) leads to $\lambda = u_p/U_\infty$ which is also finite.

If the transformed temperature profile $G'(\xi)$ is to remain finite as $\beta \to \infty$, a suitable definition for $G'(\xi)$ will be

$$\frac{\Theta_\infty - \Theta}{\Theta_p} = G'(\xi). \tag{35}$$

This requires Θ_p to be finite as $\beta \to \infty$. From (16) and (27), it can be shown that $\Theta_\tau = C\gamma\Theta_\infty$. Therefore, if Θ_p is defined as

$$\Theta_p = C\lambda\Theta_\infty \tag{36}$$

it will remain finite as $\beta \to \infty$. This suggests the following transformation for $g(\eta)$:

$$g(\eta) = G(\xi), \qquad g'(\eta) = \beta^{1/2} G'(\xi), \tag{37a,b}$$

$$\frac{\Theta_p}{\Theta_\tau} = \frac{u_p}{u_\tau} = \beta^{1/2}. \tag{37c}$$

The expressions for λ and St can now be written as

$$\frac{1}{\lambda} = \frac{1}{\kappa\beta^{1/2}} \ln\frac{U_\infty \delta^*}{\nu} + \frac{B}{\beta^{1/2}} + \frac{A}{\beta^{1/2}}, \tag{38}$$

$$St = \frac{C\lambda^2}{\beta}. \tag{39}$$

With the substitution of the transformations (32), (33) and (37), equations (30), (31) and the associated boundary conditions can be written as

$$\Phi F''-\left(\frac{1}{m}+1\right)\left[\xi F'-\left(\frac{1}{1+\lambda/\kappa\beta^{1/2}}\right)F-\lambda\left(\frac{1}{1+\lambda/\kappa\beta^{1/2}}\right)FF'+\lambda\left(\frac{1-\lambda/\kappa\beta^{1/2}}{1+\lambda/\kappa\beta^{1/2}}\right)\int_0 F'^2\,\mathrm{d}\xi\right]+2F-\lambda\int_0 F'^2\,\mathrm{d}\xi=-\frac{1}{\beta}, \quad (40)$$

$$\frac{\Phi}{Pr_t}G''-\left(\frac{1}{m}+1\right)\times\left[\xi G'-\left(\frac{1}{1+\lambda/\kappa\beta^{1/2}}\right)G-\lambda\left(\frac{1}{1+\lambda/\kappa\beta^{1/2}}\right)FG'+\lambda\left(\frac{1-\lambda/\kappa\beta^{1/2}}{1+\lambda/\kappa\beta^{1/2}}\right)\int_0 F'G'\,\mathrm{d}\xi\right]=-\frac{1}{\beta}, \quad (41)$$

$$F(0)=0, \qquad F(\xi\to\infty)=1, \qquad (42a,b)$$

$$G(0)=0, \qquad G'(\xi\to\infty)=0, \qquad (42c,d)$$

where the eddy viscosity function $\varphi(\xi)$ is defined by

$$\Phi(\xi)=\kappa^2\xi^2|F''|, \qquad \xi\leqslant E, \qquad (43a)$$

$$\Phi(\xi)=K_C, \qquad \xi\geqslant E, \qquad (43b)$$

and E is again given by the larger of the two positive roots of the equation $\kappa^2\xi^2|F''|=K_C$. Therefore, it can be seen that the equations are regular as $\beta\to\infty$ and they can be solved subject to boundary conditions (42) using conventional numerical techniques.

METHOD OF SOLUTION

Mellor and Gibson [4] suggested solving (30) and (40) by expanding f and F in terms of γ and λ, respectively, so that $f=f_0+\gamma f_1+O(\gamma^2)$ and $F=F_0+\lambda F_1+O(\lambda^2)$. Implicit in these expansions is the assumption that γ and λ are small. As a result, the equations for $f_0, f_1, F_0, F_1, \ldots$ were parametric only in β and were solved using a Runge–Kutta technique for a given β. Therefore, for a given R_{δ^*}, the velocity profiles can be calculated for any value of β. Mellor and Gibson [4] calculated the velocity profiles for the range $-0.54\leqslant\beta\leqslant\infty$ at a $R_{\delta^*}=10^5$. For ease of comparison, the present calculations are also carried out for the same range of β and R_{δ^*}.

The equations (30) and (40) can also be integrated directly without resorting to the assumption that γ and λ are small. However, iterations are required to determine the correct γ and λ for a given R_{δ^*} so that (30) and (40) are identically satisfied for a given value of β. For the present analysis, (30) and (40) are numerically integrated using a fourth-order Runge–Kutta technique to start the calculation and a predictor–corrector method is used to carry on the calculation once it has begun. It is found that the velocity solutions thus obtained agree with those reported by Mellor and Gibson [4]. However, the determined values of $A(\beta)$, $A/\beta^{1/2}$, $\tilde{G}$ and $\tilde{G}/\beta^{1/2}$ differ from those given by Mellor and Gibson [4] by about $\pm 2\%$.

In view of this, as a first guess, the equations (30), (31), (40) and (41) are solved using the values obtained by Mellor and Gibson [4] for γ and λ for the range $-0.54\leqslant\beta\leqslant\infty$. Again, the Runge–Kutta/predictor–corrector method is used to perform the integration. The logarithmic singularity for f, g, F and G at $\eta=0$ (or $\xi=0$) is avoided by starting the integration at a small value of η (or ξ), e.g. $\eta=0.00005$. To connect this limiting behavior to the physically correct behavior, $U\to 0$, $\Theta\to 0$ as $\eta\to 0$, the skin friction and the Stanton number relations (20), (29), (38) and (39) are used. A detailed discussion of the determination of C (β, Pr_t) is given below.

THE MEAN TEMPERATURE PROFILES

The complete solution for the velocity profiles at different values of β and $R_{\delta^*}=10^5$ has been given by Mellor and Gibson [4]. In addition, they have reported the variations of A, $\tilde{G}$ and γ with β and the variation of γ with R_{δ^*}. In view of this, only the calculated mean temperature profiles are presented here. Two different sets of temperature profiles for the range $-0.5\leqslant\beta\leqslant\infty$ are shown; one for $Pr_t=0.7$ and another for $Pr_t=1.0$. The plots for $Pr_t=1.0$ are given in Figs. 1 and 2 while those for $Pr_t=0.7$ are shown in Figs. 3 and 4. From these results, it can be seen that an overlap exists between the inner and outer layer and this leads to a logarithmic region for the profiles of g' and G' for all values of β except $\beta\to\infty$. More will be said about the profile for the $\beta\to\infty$ case later. The logarithmic portion of the profile is described by

$$g'=-\frac{1}{\kappa_\theta}\ln\eta+A_\theta(\beta,Pr_t), \qquad (44)$$

or

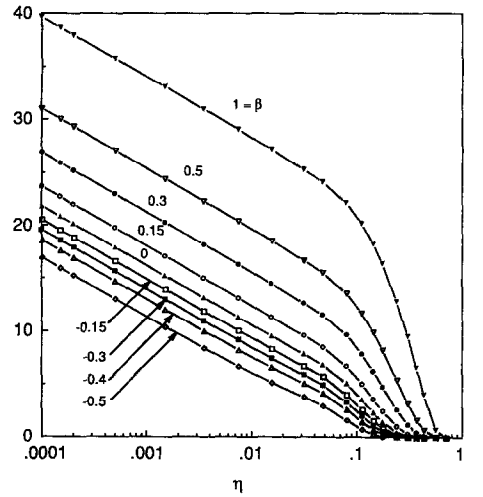

FIG. 1. Calculated defect temperature profiles for small β and $Pr_t=1$.

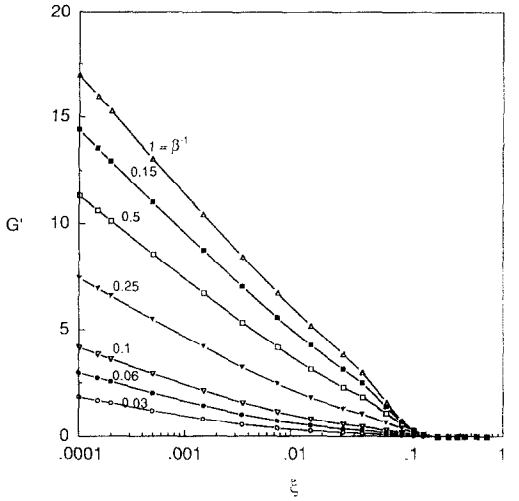

FIG. 2. Calculated defect temperature profiles for large β and $Pr_t = 1$.

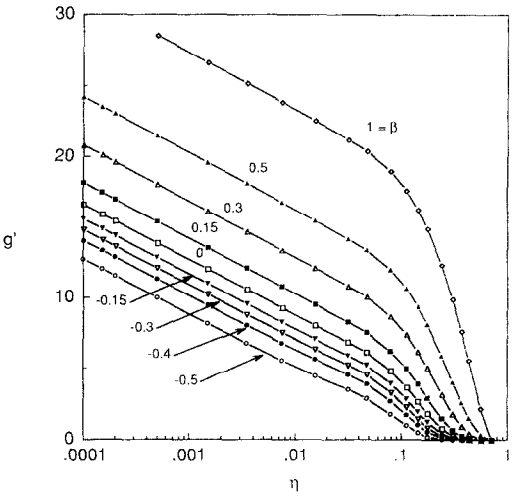

FIG. 3. Calculated defect temperature profiles for small β and $Pr_t = 0.7$.

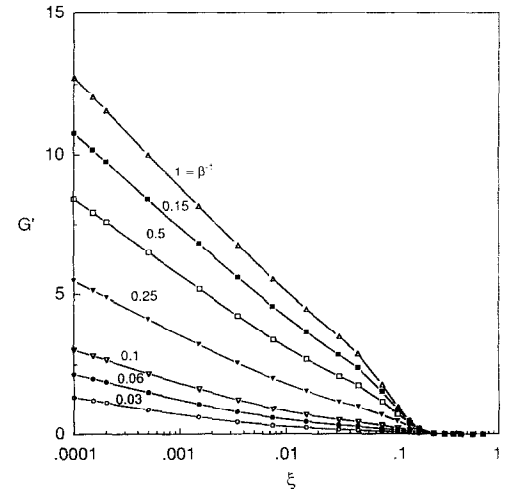

FIG. 4. Calculated defect temperature profiles for large β and $Pr_t = 0.7$.

$$G' = -\frac{1}{\kappa_\theta \beta^{1/2}} \ln\left(\frac{\xi}{\beta^{1/2}}\right) + \frac{A_\theta(\beta, Pr_t)}{\beta^{1/2}}. \quad (45)$$

The slope of the logarithmic region shown in Figs. 1–4 can now be determined. Values thus obtained for κ_θ are 0.410 and 0.586 for the cases with $Pr_t = 1$ and 0.7, respectively, and show that the relation $\kappa_\theta = \kappa/Pr_t$ is indeed valid.

Values of A_θ and $A_\theta/\beta^{1/2}$ determined from these plots are tabulated in Tables 1(a) and (b), respectively, together with the values of A which agree to within $\pm 2\%$ of those given by Mellor and Gibson [4]. In Tables 1(a) and (b), the values of A_θ and $A_\theta/\beta^{1/2}$ for selected values of β and for $Pr_t = 0.85$, 2, 4 and 7 are also listed. A plot of A_θ and $A_\theta/\beta^{1/2}$ vs β for two different values of Pr_t is given in Fig. 5, while a plot of A_θ vs Pr_t for several values of β is shown in Fig. 6. The dashed lines shown in Fig. 5 represent the extrapolation of $A_\theta/\beta^{1/2}$ to zero as $\beta \to \infty$ (or $\beta^{-1} \to 0$). These results clearly show the dependence of A_θ on β and Pr_t.

It should be noted that (30) and (31) are identical equations for the case $\beta = 0$ and $Pr_t = 1$. The boundary conditions for both equations are the same because (27b) is equivalent to the condition $f'(\eta \to \infty) = 0$. Therefore, the solutions for f' and g are identical. This fact led Back and Cuffel [23] to plot their mean velocity and mean temperature profiles in the form of Θ/Θ_c vs U/U_c for accelerated boundary layers. Thus, any deviation of the profile from the straight line behavior will be clearly illustrated. The effects of negative and positive pressure gradient on boundary-layer flows can again be illustrated by plotting Θ/Θ_c vs U/U_c. In the present nomenclature, they are equivalent to plotting $1 - g/g'(0)$ vs

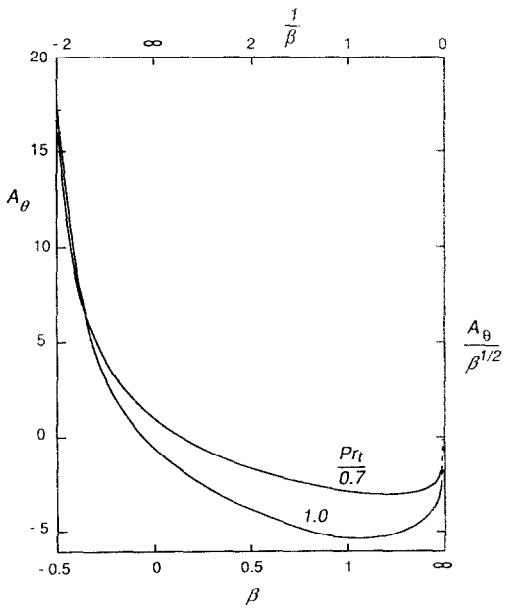

FIG. 5. Variations of A_θ and $A_\theta/\beta^{1/2}$ with β for two values of Pr_t.

Table 1.

(a) Values of A_θ determined at $R_{\delta^*} = 10^5$ for different values of Pr_t and $\beta \leqslant 1$

Pr_t		0.7	0.85	1	2	4	7
β	A			A_θ			
−0.5	−2.58	15.50		17.20			
−0.4	−2.17	8.48		8.56			
−0.3	−1.76	5.08		4.44	0.26	−12.30	−35.70
−0.15	−1.17	2.45		1.25			
0	−0.60	0.94	0.21	−0.60	−0.73	−23.90	−52.80
0.15	−0.07	−0.09		−1.87			
0.3	0.44	−0.85		−2.81			
0.5	1.08	−1.62		−3.76	−12.20	−31.80	−64.80
1	2.55	−2.92		−5.40	−14.70	−36.00	−71.30

(b) Values of $A_\theta/\beta^{1/2}$ determined at $R_{\delta^*} = 10^5$ for different values of Pr_t and $1/\beta \leqslant 1$

Pr_t			0.7	0.85	1	2	4	7
$1/\beta$	β	$A/\beta^{1/2}$			$A_\theta/\beta^{1/2}$			
1	1	2.55	−2.92		−5.40	−14.70	−36.00	−71.30
0.75	1.33	2.99	−3.02		−5.31			
0.5	2	3.59	−3.06		−5.09			
0.25	4	4.60	−2.93		−4.59	−10.50	−23.60	−44.70
0.1	10	5.77	−2.50		−3.76	−8.16	−17.60	−32.60
0.06	16.67	6.33	−2.21		−3.28			
0.03	33.33	6.98	−1.82		−2.66			
0	∞	10.27						

$1-f'/f'(0)$ or $1-G'/G'(0)$ vs $1-F'/F'(0)$. Selected profiles are shown in Figs. 7 and 8 for the $Pr_t = 1$ and $Pr_t = 0.7$ cases, respectively. The behavior of the accelerated equilibrium boundary layers is similar to those shown by Back and Cuffel [23]; namely that the mean temperature profiles lie below the mean velocity profiles at a given distance from the wall. For decelerated equilibrium boundary layers, the opposite trend is observed; that is, at a given distance from the wall, the mean temperature profiles lie above the mean

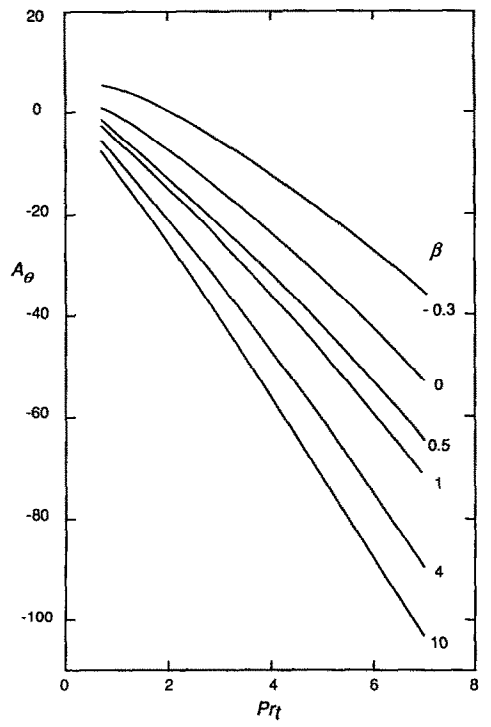

FIG. 6. Variations of A_θ with Pr_t for different values of β.

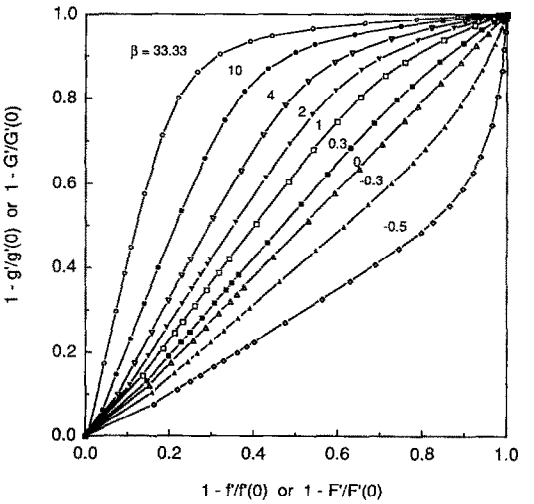

FIG. 7. A plot of the mean temperature profiles vs the mean velocity profiles for different values of β and $Pr_t = 1$.

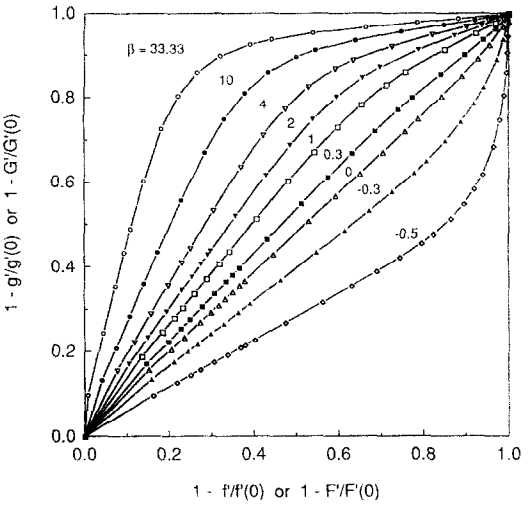

FIG. 8. A plot of the mean temperature profiles vs the mean velocity profiles for different values of β and $Pr_t = 0.7$.

velocity profiles. As β increases, the curve becomes more and more like an inverted L. This behavior simply reflects the rapid decrease of the mean velocity compared to the mean temperature as incipient separation is approached.

The temperature profile $G'(\xi)$ in the limit of $\beta \to \infty$ can be determined by examining (41). As $\beta \to \infty$, $1/\beta \to 0$, therefore (41) becomes homogeneous. Since the boundary conditions (42c,d) are also homogeneous, the only valid solutions for $G(\xi)$ and $G'(\xi)$ are that they are zero everywhere. This means that, in the limit $\beta \to \infty$, $\Theta = \Theta_\infty$ everywhere outside the near-wall region and the temperature increase from 0 to Θ_∞ occurs in the thermal sublayer. Therefore, $A_\theta/\beta^{1/2}$ approaches zero as $\beta \to \infty$ for all values of Pr_t. Since the present analysis neglects the effects of viscosity by assuming the Reynolds number to be very large, there is no need to specify a Prandtl number. Consequently, the thickness of the thermal sublayer cannot be determined and the gradient of Θ at the wall is not known. This gives rise to an undetermined wall heat flux in the limit of $\beta \to \infty$. Even though this represents a shortcoming in the present analysis, it can be easily remedied by including the viscous sublayer in the analysis, much like that outlined by Mellor [5].

For the case $\beta = 0$ and $Pr_t = 1$, the solutions for f and g are identical. Since g' for the $\beta = 0$ case can be represented either by (4) or (44), then

$$\tilde{A}_\theta = A_\theta + \frac{1}{\kappa_\theta} \ln\left(\frac{\Delta}{\delta}\right). \tag{46}$$

The dimensionless thermal boundary layer thickness (η_δ) for this case can be determined from the condition: $\Theta(\eta_\delta) = 0.99\Theta_\infty$. This gives $\eta_\delta = \delta/\Delta = 0.4$. Using $A_\theta = -0.6$, (46) gives $\tilde{A}_\theta = 1.63$. On the other hand, if $Pr_t = 0.85$ is assumed in accordance with the analysis of Kader and Yaglom [10], then $\eta_\delta = 0.4$ again, while $A_\theta = 0.21$ and $\tilde{A}_\theta = 2.11$. The approximate value assumed by Kader and Yaglom [10] and later by Yaglom [13] is $\tilde{A}_\theta = 2.35$. This is in good agreement with the value of $\tilde{A}_\theta$ determined from the present analysis. The effect of $\tilde{A}_\theta$ on the calculated Stanton number is examined in the next section.

Finally, the dimensionless heat flux $(\varphi/Pr_t)g''$ and $(\Phi/Pr_t)G''$ for the case $Pr_t = 1.0$ are plotted in Figs. 9 and 10, respectively. Since the heat flux profiles for other values of Pr_t are similar to those shown, they will not be presented here. Unlike the shear stress profiles whose maxima move away from the wall as β increases [4], the maxima of the heat flux profiles remain at the wall. This is a consequence of the fact that the pressure gradient does not have a direct effect on the temperature field, only an indirect effect through the interaction of the velocity field.

THE MODIFIED REYNOLDS ANALOGY

Near the wall, the flow is solely determined by local properties and is independent of the freestream conditions. Consequently, the temperature profile for this region is given by the logarithmic law of the wall (1) and is independent of the pressure gradient. Far away from the wall, the defect temperature profile is given by (44). The existence of an overlap between (1) and (44) allows $\Theta_\infty/\Theta_\tau$ to be determined. If use is made of (16) and the definition (29) for St, it can be shown that

$$\frac{\Theta_\infty}{\Theta_\tau} = \frac{1}{C_f^{1/2}} = \frac{1}{\kappa_\theta} \ln\left(\frac{U_\infty \delta^*}{\nu}\right) + B_\theta + A_\theta(\beta, Pr_t). \tag{47}$$

In obtaining (47), use has been made of the identity $u_\tau \Delta = U_\infty \delta^*$. An expression for C can now be obtained by combining (47) with (20). The result is

$$C = \frac{\kappa^{-1} \ln R_{\delta^*} + B + A(\beta)}{\kappa_\theta^{-1} \ln R_{\delta^*} + B_\theta + A_\theta(\beta, Pr_t)}. \tag{48}$$

For large β, the corresponding expression for C becomes

$$C = \frac{\kappa^{-1}\beta^{-1/2} \ln R_{\delta^*} + B\beta^{-1/2} + A(\beta)\beta^{-1/2}}{\kappa_\theta^{-1}\beta^{-1/2} \ln R_{\delta^*} + B_\theta\beta^{-1/2} + A_\theta(\beta, Pr_t)\beta^{-1/2}}. \tag{49}$$

Values of C are calculated for $R_{\delta^*} = 10^5$ and based on $\kappa = 0.41$, $\kappa_\theta = \kappa/Pr_t$, $B = 4.9$, $B_\theta = 3.8$ and values of A, $A/\beta^{1/2}$, A_θ and $A_\theta/\beta^{1/2}$ as tabulated in Table 1. They are listed in Tables 2(a) and (b) for values of $\beta \leqslant 1$ and $\beta \geqslant 1$, respectively, and are also plotted in Fig. 11 with C vs β and Fig. 12 with C vs Pr_t to show the dependence of C on β and Pr_t. For accelerated flows, the values of C are determined to be less than 1 for the $Pr_t = 1$ case. These values are consistent with values of ~ 0.7 to ~ 0.75 measured at a location outside of the viscous sublayer by Back and Cuffel [23, 24] in an accelerating flow through a convergent–divergent nozzle. Therefore, the measurements lend credence to the present analysis. However, the impor-

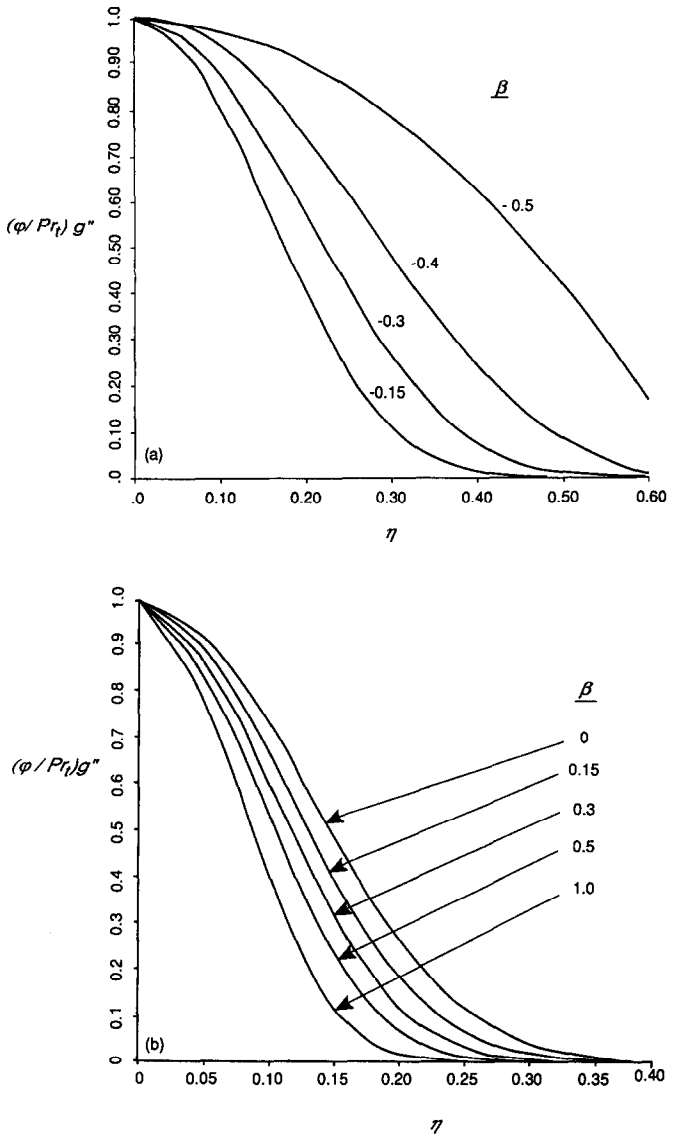

FIG. 9. Calculated heat flux profiles for small β and $Pr_t = 1$; (a) $\beta < 0$, (b) $\beta > 0$.

tant result of the present analysis is the predicted trend of C which decreases in accelerated turbulent boundary layers and increases in adverse pressure gradient flows.

From Tables 2(a) and (b), it is obvious that C changes rapidly as Pr_t varies. On the other hand, the effect of Pr_t on the predicted mean profiles is not as clearly illustrated in Figs. 9 and 10. Another way to examine this effect more critically is to plot the mean temperature vs the mean velocity for different values of Pr_t at a given value of β. Since Pr_t cannot differ too much from 1, these plots should be limited to values of Pr_t ranging from 0.7 to 2. Three sets of sample plots are shown in Figs. 13–15 for $\beta = -0.3$, 0 and 1, respectively. In all three pressure gradient cases, the effect of Pr_t on the profile shape is minimal for $Pr_t \leqslant 1$. In other words, as far as the calculations of the mean profiles are concerned, a slight change in Pr_t has little effect on their predicted shapes. However, the calculated C could be off by 10% or more. This suggests that a proper choice for Pr_t is obtained by matching St rather than by matching the mean profiles.

In the limit $\beta \to \infty$, $G'(\xi)$ goes to zero everywhere outside of the near-wall layer. This leads to the disappearance of the logarithmic behavior in the defect profile and hence the overlap with the law of the wall. As a result, C cannot be determined for this limiting case. However, this does not represent a shortcoming of the present analysis. As mentioned previously, the wall heat flux cannot be determined in the limit of $\beta \to \infty$ because viscous effects are neglected in the present formulation. Therefore, St is unknown and C cannot be evaluated. A remedy is to include the viscous sublayer in the formation along the line proposed by Mellor [5].

It is of interest to note that the classical Reynolds

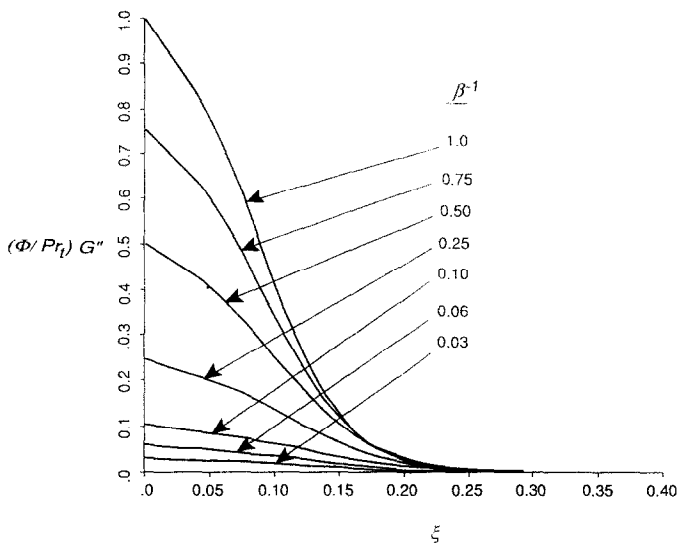

FIG. 10. Calculated heat flux profiles for large β and $Pr_t = 1$.

analogy is not exactly correct even for the case $\beta = 0$ and $Pr_t = 1$ (see Tables 2(a) and (b)). However, as $R_{\delta^*} \to \infty$, $C \to \infty$, $C \to (1/Pr_t)$ for all values of β. Therefore, the classical Reynolds analogy is valid only in the limit of $Pr_t \to 1$ and $R_{\delta^*} \to \infty$.

DISCUSSION

There are essentially very few data available for the validation of (48) and (49) for finite values of β. However, part validation of (48) could be achieved by comparing it with data in the literature [8, 9, 25–27].

Reynolds *et al.* [8] and Perry *et al.* [9] studied heat transfer on a flat plate ($\beta = 0$). They reported measurements of both skin friction coefficient and Stanton number. If (48) is re-written in terms of the skin friction coefficient, the expression for the Stanton number becomes

Table 2.

(a) Values of C determined at $R_{\delta^*} = 10^3$ for different values of Pr_t and $\beta \leqslant 1$

	Pr_t	0.7	0.85	1	2	4	7
β	A			C			
−0.5	−2.58	0.78		0.62			
−0.4	−2.17	0.97		0.76			
−0.3	−1.76	1.09		0.86	0.52	0.30	0.19
−0.15	−1.17	1.23		0.96			
0	−0.60	1.33	1.16	1.04	0.62	0.35	0.22
0.15	−0.07	1.41		1.10			
0.3	0.44	1.48		1.15			
0.5	1.08	1.56		1.21	0.71	0.40	0.25
1	2.55	1.73		1.34	0.79	0.44	0.28

(b) Values of C determined at $R_{\delta^*} = 10^3$ for different values of Pr_t and $1/\beta \leqslant 1$

	Pr_t		0.7	0.85	1	2	4	7
$1/\beta$	β	$A/\beta^{1/2}$			C			
1	1	2.55	1.73		1.34	0.79	0.44	0.28
0.75	1.33	2.99	1.82		1.42			
0.5	2	3.59	1.99		1.54			
0.25	4	4.60	2.40		1.86	1.08	0.61	0.38
0.1	10	5.77	3.29		2.56	1.50	0.85	0.53
0.06	16.67	6.33	4.08		3.18			
0.03	33.33	6.98	5.66		4.44			
0	∞	10.27						

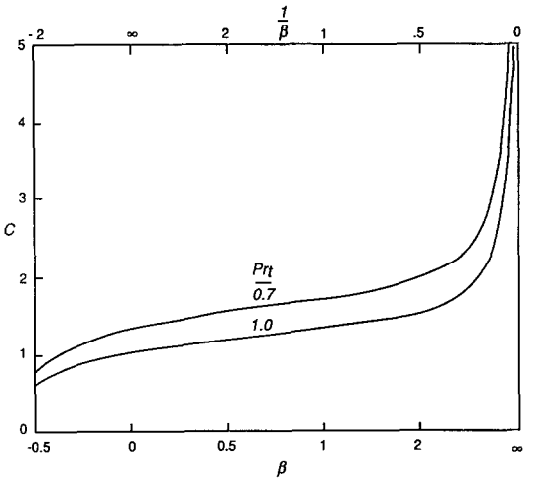

FIG. 11. Variations of C with β for two values of Pr_t.

$$St = \frac{(C_f/2)^{1/2}}{(\kappa/\kappa_\theta)[(2/C_f)^{1/2} - A - B] + B_\theta + A_\theta}. \quad (50)$$

Therefore, St can be calculated once C_f is known. Taking $Pr_t = 0.85$ as suggested by Kader and Yaglom [10] for flat boundary layers, (50) is used to evaluate St based on the calculated C_f. The calculated results for C_f are 0.00330 for Reynolds *et al.*'s [8] experiment and 0.00300 for Perry *et al.*'s [9] experiment. The corresponding measured values are 0.00330 and 0.00300, respectively. As for St, the measured values are 0.00190 and 0.00180, respectively, for the experiments of Reynolds *et al.* and Perry *et al.* The corresponding predictions are 0.00191 and 0.00176, respectively. According to Perry *et al.* [9], the accuracy of the St measurements is $\pm 7\%$ of the reported value. Consequently, it can be said that the calculated values are in good agreement with measured data.

The flat plate boundary-layer data [25–27] have been analysed carefully by Kader and Yaglom [10]. They found that the Nusselt number Nu deduced from the data correlates well with the equation

$$Nu = \frac{Re_x C_f^{1/2}}{1.714(2/C_f)^{1/2} - 0.275}, \quad (51)$$

where $Pr = 0.7$ has been assumed for air. A similar expression can be deduced for Nu if use is made of (20), (29) and (48). The result, after the constant values of $A = -0.6$, $B = 4.9$, $B_\theta = 3.8$ and $A_\theta = 0.21$ have been substituted, is

$$Nu = \frac{Re_x C_f^{1/2}}{2.02 Pr_t (2/C_f)^{1/2} - 8.688 Pr_t + 8.093}. \quad (52)$$

Again $Pr = 0.7$ is assumed for air. It can be seen that if $Pr_t = 0.85$ is used, $2.02 Pr_t$ takes on a value of 1.717, which is about the same as that given in (51). However, $(8.093 - 8.688 Pr_t) = 0.708$, which is not equal to that given in (51). A plot of (51) and (52) is shown in Fig. 16. The close agreement between the two expressions lends credence to the present analysis. It should be pointed out that A_θ and B_θ are parametric in Pr. Therefore, (52) is also valid for other values of Pr much like the empirical expression (51) derived by Kader and Yaglom [10].

The DNS data reported by Kim and Moin [16], by Kasagi *et al.* [17] and by Kasagi and Ohtsubo [18] are for a bulk Reynolds number less than 6600. Therefore, viscous effects are important and cannot be neglected. In view of this, it is not appropriate to compare the present analysis with the DNS data. However, the DNS results are found to agree well with the empirical mean temperature profiles of Kadar [28] at about the same Reynolds number. Since Kader's [28] empirical results and the present results are in good agreement with the similarity analysis of Yaglom [13], it can be inferred that the present results are also in good agreement with DNS data at the same Reynolds number.

Finally, it should be noted that the present analysis is applicable to turbulent flow with wall mass transfer under equilibrium conditions. This follows directly from equation (7) which is also valid for mass transfer problems provided Θ is interpreted to denote the mix-

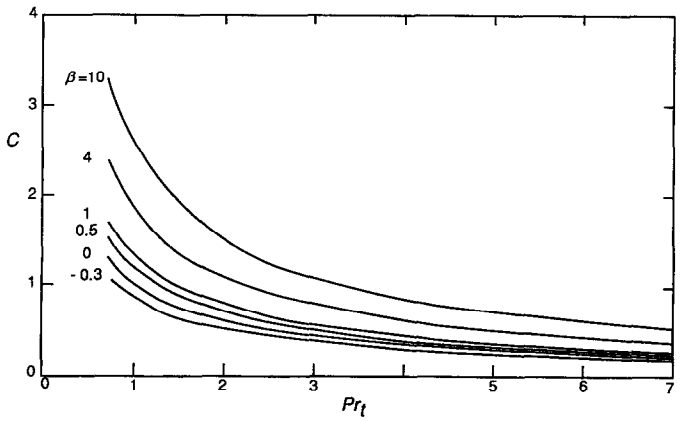

FIG. 12. Variations of C with Pr_t for different values of β.

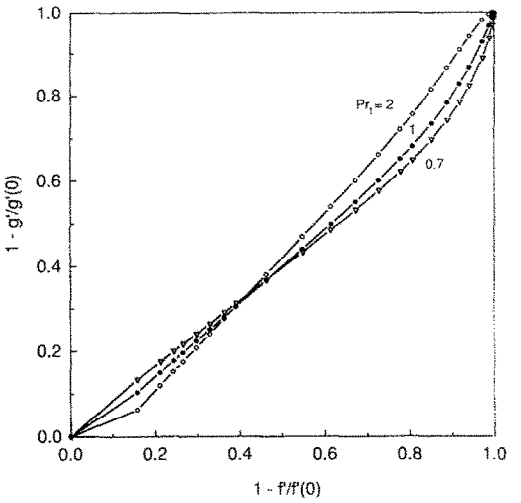

FIG. 13. A plot of the mean temperature profiles vs the mean velocity profiles for different values of Pr_t and $\beta = -0.3$.

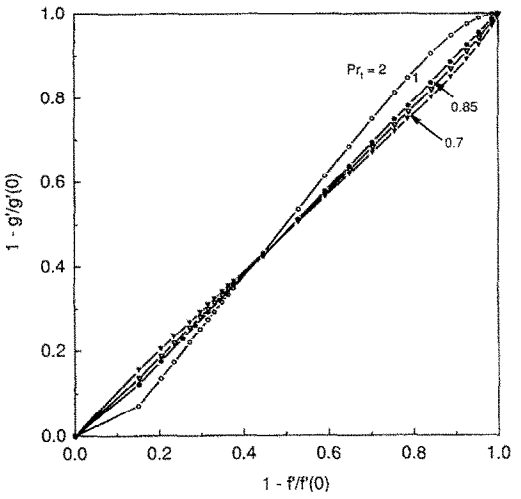

FIG. 14. A plot of the mean temperature profiles vs the mean velocity profiles for different values of Pr_t and $\beta = 0$.

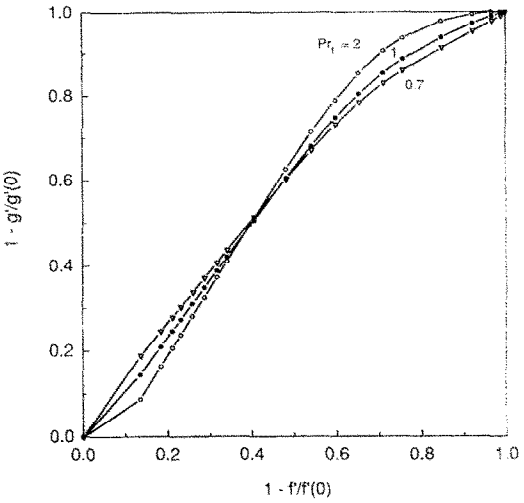

FIG. 15. A plot of the mean temperature profiles vs the mean velocity profiles for different values of Pr_t and $\beta = 1$.

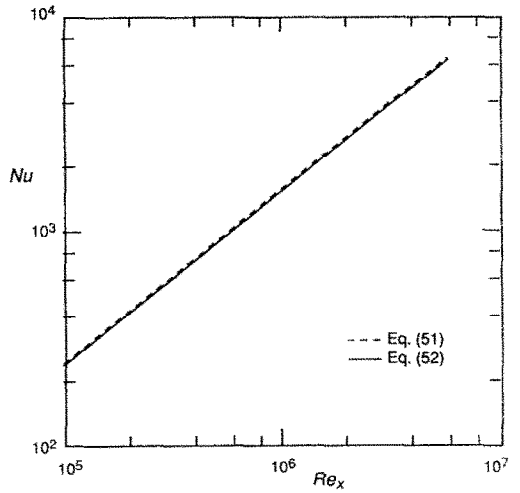

FIG. 16. A plot of Nu vs Re_x for $\beta = 0$ and $Pr_t = 0.85$.

ture mass fraction. Furthermore, the mixture mass fraction can be normalised to zero at the wall and unity in the free stream. Under these conditions, (10c) represents the mass flux at the wall and the governing equations and boundary conditions are identical to the heat transfer problem treated here.

CONCLUSIONS

Incompressible, equilibrium turbulent thermal boundary layers, characterised by β = constant, have been analysed. A family of defect temperature profiles parametric in both β and Pr_t has been obtained for the permissible range, $-0.54 \leqslant \beta \leqslant \infty$; corresponding to turbulent boundary layers with a favorable pressure gradient beyond which no equilibrium flow exists and turbulent flows at incipient separation, respectively. From these results, a modified Reynolds analogy defining the relation between St and C_f has been deduced. The proportionality constant C thus deduced is shown to be parametric in both β and Pr_t. For a given Pr_t, C decreases as β decreases and increases when the pressure gradient becomes increasingly adverse. On the other hand, when β is kept constant, C decreases with increasing Pr_t. These trends are true for all values of β and Pr_t examined. The present results lead to the conclusion that the classical Reynolds analogy is correct only in the limit of $\beta = 0$, $Pr_t \to 1$ and $R_{\delta^*} \to \infty$. It is further shown that the Stanton and Nusselt numbers thus deduced are in good agreement with measured data obtained in air. Finally, it is pointed out that the present analysis can be used to study equilibrium turbulent flows with mass transfer at the wall.

REFERENCES

1. F. Clauser, The turbulent boundary layer, *Adv. Appl. Mech.* **4,** 1–51 (1956).
2. A. A. Townsend, The properties of equilibrium boundary layers, *J. Fluid Mech.* **1,** 561–573 (1956).
3. A. A. Townsend, Equilibrium layers and wall turbulence, *J. Fluid Mech.* **11,** 97–120 (1961).
4. G. L. Mellor and D. M. Gibson, Equilibrium turbulent boundary layers, *J. Fluid Mech.* **24,** 225–253 (1966).
5. G. L. Mellor, The effects of pressure gradients on the flow near a smooth wall, *J. Fluid Mech.* **24,** 255–274 (1966).
6. B. S. Stratford, An experimental flow with zero skin friction throughout its region of pressure rise, *J. Fluid Mech.* **5,** 17–35 (1959).
7. S. J. Kline, W. C. Reynolds, F. A. Schraub and P. W. Runstadler, The structure of turbulent boundary layers, *J. Fluid Mech.* **30,** 741–773 (1967).
8. W. C. Reynolds, W. M. Kays and S. J. Kline, Heat transfer in the turbulent incompressible boundary layer. I—Constant wall temperature, *NASA Tech. Memo.* 12-1-58W (1958).
9. A. E. Perry, J. B. Bell and P. N. Joubert, Velocity and temperature profiles in adverse pressure gradient turbulent boundary layers, *J. Fluid Mech.* **25,** 299–320 (1966).
10. B. A. Kader and A. M. Yaglom, Heat and mass transfer laws for fully turbulent wall flows, *Int. J. Heat Mass Transfer* **15,** 2329–2351 (1972).
11. E. Brundrett and P. R. Burroughs, The temperature inner-law and heat transfer for turbulent air flow in a vertical square duct, *Int. J. Heat Mass Transfer* **10,** 1133–1142 (1967).
12. A. E. Perry and P. H. Hoffmann, An experimental study of turbulent convection heat transfer from a flat plate, *J. Fluid Mech.* **77,** 355–368 (1976).
13. A. M. Yaglom, Similarity laws for constant-pressure and pressure-gradient turbulent wall flows, *Ann. Rev. Fluid Mech.* **11,** 505–540 (1979).
14. P. M. Moretti and W. M. Kays, Heat transfer to a turbulent boundary layer with varying free-stream velocity and varying temperature—an experimental study, *Int. J. Heat Mass Transfer* **8,** 1187–1202 (1965).
15. L. H. Back and R. A. Seban, On constant property turbulent boundary layers with variable temperature or heat flow at the wall, *J. Heat Transfer* **87,** 151–156 (1965).
16. J. Kim and P. Moin, Transport of passive scalars in a turbulent channel flow. In *Turbulent Shear Flows* 6 (Edited by Andre *et al.*), pp. 85–96. Springer, Berlin (1989).
17. N. Kasagi, Y. Tomita and A. Kuroda, Direct numerical simulation of the passive scalar field in a two-dimensional turbulent channel flow, *Proceedings of the 3rd ASME–JSME Thermal Engineering Joint Conference*, Reno, Vol. 3, pp. 175–182 (1991); also to appear in *J. Heat Transfer*.
18. N. Kasagi and Y. Ohtsubo, Direct numerical simulation of low Prandtl number thermal field in a turbulent channel flow. In *Turbulent Shear Flows* 8 (Edited by Durst *et al.*), pp. 97–119. Springer, Berlin (1992).
19. M. Hishida, Y. Nagano and M. Tagawa, Transport process of heat and momentum in the wall region of turbulent pipe flow, *Proceedings of the 8th International Heat Transfer Conference*, Vol. 3, pp. 925–930 (1986).
20. W. M. Kays, *Convective Heat and Mass Transfer*, pp. 151–155. McGraw-Hill, New York (1966).
21. J. A. Businger, J. C. Wyngaard, Y. Izumi and E. F. Bradley, Flux-profile relationships in the atmospheric surface layer, *J. Atmos. Sci.* **28,** 181–189 (1971).
22. S. P. S. Arya, Buoyancy effects in a horizontal flat-plate boundary layer, *J. Fluid Mech.* **68,** 321–343 (1975).
23. L. H. Back and R. F. Cuffel, Relationship between temperature and velocity profiles in a turbulent boundary layer along a supersonic nozzle with heat transfer, *AIAA J.* **8,** 2066–2069 (1970).
24. L. H. Back and R. F. Cuffel, Turbulent boundary layer and heat transfer measurements along a convergent–divergent nozzle, *J. Heat Transfer* **93,** 397–407 (1971).
25. A. A. Slanciauskas, R. V. Ulinskas and A. A. Zukauskas, Turbulent heat transfer from a flat plate to liquids of variable viscosity, *Trudy. Akad. Nauk. Lithuan. SSR* **4B,** 163–178 (1969).
26. B. S. Petrekhov, A. A. Detlaf and V. V. Kirillov, Experimental investigation of the local heat transfer from a plate in subsonic turbulent air flow, *Zh. Tekhn. Fiz.* **24,** 1761–1772 (1954).
27. E. Achenbach, Betrag zur Messung der Örtlichen Wärmeübergangszahl in turbulenten Reibungsschichten bei erzwungener Konvektion, *Glastechn. Ber.* **39,** 217–225 (1966).
28. B. A. Kader, Temperature and concentration profiles in fully turbulent boundary layers, *Int. J. Heat Mass Transfer* **24,** 1541–1544 (1981).